

The Determination of Sea Surface Temperature from AVHRR Infrared Data in Cloudy Area

Gin-Rong Liu and Sally Tang
Center for Space and Remote Sensing Research
National Central University
Chung-Li, Taiwan, R.O.C.

Commission VII

Abstract

A multiple-channel method is developed to determine sea surface temperature from the radiation measurements of AVHRR infrared window channels. To estimate sea surface temperature from satellite observed infrared window channel radiances, it has been necessary to first select or determine the radiances for clear air. In this study, a simple and accurate cloud-clearing technique called "spatial coherence method" is applied to extract the clear air radiances from observed cloud-contaminated radiances.

The results obtained from this method are compared with conventional ship observations. The intercomparisons reveal the usefulness of this technique in estimating sea surface temperature in cloudy area.

1. Introduction

Because of their influence on the energy transfer between the ocean and the atmosphere, the sea surface temperature (SST) has received significant attention for many decades. The results of satellite-derived SST were encouraging in numerous research (Smith et al., 1970; Warnecke et. al., 1971; Prabhakara et. al., 1974; Bates, 1982). The great advantage of using two or more infrared window regions than a single one is that the effect of water vapor attenuation along the path can be directly accounted for. Using multispectral data to determine SST, the results in comparing with buoy/ship measurements are showing a low bias and root mean square error (RMSE) of approximately 1°C (McClain, 1980).

To derive SST from satellite observed infrared window channel radiances, it has necessary to use the radiances of clear air. Otherwise, the cloud effect will causes a large error in determining SST. The study conducted here focuses on achieving similar SST accuracy in the cloud-contaminated areas.

The NOAA (National Oceanic and Atmospheric Administration) polar orbiting satellites provide 1 Km resolution AVHRR (Advanced Very High Resolution Radiometer) data, which are useful for searching clear spots in the partly cloudy areas. The AVHRR has 5 channels in the visible, near-infrared and infrared. Characteristics of AVHRR channels are given in Table 1.

2. Multichannel SST algorithm

The radiative transfer equation at a fixed observing zenith angle can be written as

$$I(\nu) = B_s \tau_s - \int_0^{P_s} B[\nu, T(p)] d\tau(\nu, p) \quad (1)$$

where I , B , and τ are the satellite observed radiance, Planck radiance, and atmospheric transmittance, respectively. ν is wavenumber, and $T(p)$ is temperature at pressure level p . The subscript s indicates the surface condition. In the infrared window regions, the absorption is weak and may use the assumption

$$\tau(\nu, U) = \text{EXP}(-K(\nu)U) \simeq 1 - K(\nu)U$$

$$d\tau(\nu, U) \simeq -K(\nu)U$$

where U and $K(\nu)$ are the precipitable water vapor and absorption coefficient, respectively. So that (1) becomes

$$I(\nu) = B_s(1 - K(\nu)U_s) + K(\nu) \int_0^{U_s} B[\nu, T(p)] dU \quad (2)$$

Defining an atmospheric mean Planck radiance B_m as

$$B_m = \int_0^{U_s} B dU / \int_0^{U_s} dU = \int_0^{U_s} B dU / U_s$$

Then

$$I(\nu) = B_s(1 - K(\nu)U_s) + K(\nu)B_m U_s$$

or

$$B_s - I(\nu) = (B_s - B_m)K(\nu)U_s \quad (3)$$

Since $B_s \approx I(\nu)$ and $B_m \approx B_s$, the first order Taylor expansion can be applied

$$B_s - I(\nu) \approx (\partial B / \partial T)_s (T_s - T_b) \quad (4)$$

$$B_s - B_m \approx (\partial B / \partial T)_s (T_s - T_m) \quad (5)$$

Substituting (4) and (5) into (3) yields

$$T_s - T_b = (T_s - T_m)K(\nu)U_s \quad (6)$$

If one consider two window channels, ν_1 and ν_2 , then

$$(T_s - T_b(\nu_1)) / (T_s - T_b(\nu_2)) = K(\nu_1) / K(\nu_2) = K_1 / K_2$$

or

$$T_s = \frac{K_2}{K_2 - K_1} T_b(\nu_1) - \frac{K_1}{K_2 - K_1} T_b(\nu_2) \quad (7)$$

Rearranging (7) yields

$$T_s = T_b(\nu_1) + \frac{K_1}{K_2 - K_1} (T_b(\nu_1) - T_b(\nu_2)) \quad (8)$$

Likewise, for Three window channels

$$T_s = T_b(\nu_1) + \frac{K_1}{2(K_2 - K_1)} (T_b(\nu_1) - T_b(\nu_2)) + \frac{K_1}{2(K_3 - K_1)} (T_b(\nu_1) - T_b(\nu_3)) \quad (9)$$

In practice, one can express the multichannel SST algorithm as

$$T_s = A_0 + \sum_{i=1}^n A_i T_b(\nu_i) \quad (10)$$

where n is the number of window channels. In Taiwan area, Tseng (1986) had used three month radiosonde data (from October to December, 1986) and applied LOWTRAN-6 to simulate AVHRR brightness temperature. He combined these brightness temperature and ship observed SST to estimate the coefficients of Eq.(10). The results are shown in Table 2.

3. Cloud-clearing Technique

The method of Multichannel SST determination requires that only cloud-free radiances be used. Thus, it is necessary to extract clear air radiances from areas that are partly cloudy. In this study, we apply the spatial coherence method (Coakley and Bretherton, 1982) which originally used to estimate cloud cover, to extract the clear air brightness temperature.

Figure 1.a shows the frequency histogram of the observed AVHRR Channel 4 brightness temperature for a .5 latitude by .5 longitude region. Within this region, the local mean and standard deviation of brightness temperature calculated for every 2X2 array of adjacent spots. Figure 1.b shows the local standard deviation of AVHRR Channel 4 brightness temperature as a function of the local mean brightness temperature. The cluster of low local standard deviation points at the warm temperature is interpreted as representing the brightness temperature of cloud-free spots. The cluster of low local standard deviation points at the cold temperature is interpreted as representing the brightness temperature of completely cloudy spots. Thereafter, we use .5 as the cut-off to the local standard deviation. That is, only the point its local standard deviation is smaller than .5 can be remained (see Figure 1.c). After reconstructing the frequency histogram of these points, two separate modes will be shown (see Figure 1.d). The warm temperature mode represents the cloud-free spots and we assume its distribution is Gaussian. That is, it has a normal density function of the form

$$f(T_b) = f_0 \text{EXP}(- (T_b - T_{b0})^2 / 2\sigma^2) \quad (11)$$

where f is the frequency of occurrence, σ is the standard deviation, and the mean brightness temperature T_{b0} is the quantity sought. From (11), it follows that any three points (T_{bi} , T_{bj} , and T_{bk}) that are part of a normal distribution satisfy the three equations

$$\begin{aligned} f_i &= f_0 \text{EXP}(- (T_{bi} - T_{b0})^2 / 2\sigma^2) \\ f_j &= f_0 \text{EXP}(- (T_{bj} - T_{b0})^2 / 2\sigma^2) \\ f_k &= f_0 \text{EXP}(- (T_{bk} - T_{b0})^2 / 2\sigma^2) \end{aligned}$$

and can be solved for T_{b0} as

$$T_{b0} = \frac{T_{bi}^2 \ln(f_j/f_k) - T_{bj}^2 \ln(f_i/f_k) + T_{bk}^2 \ln(f_i/f_j)}{2(T_{bi} \ln(f_j/f_k) - T_{bj} \ln(f_i/f_k) + T_{bk} \ln(f_i/f_j))} \quad (13)$$

Applying this procedure for AVHRR Channel 3, 4 and 5, one can have the clear air brightness temperature of Channel 3, 4 and 5 for the region contaminated by cloud.

4. Results

Figure 2.a shows images constructed from the AVHRR Channel 4

radiances observed for a region from 20N to 28N and from 118E to 127E at 07Z on December 21, 1987. One can see that this image is almost covered by cloud except a narrow clear band along China coast-line. The southern part of this region is almost overcast that may be impossible to extract clear air radiances to estimate SST. Figure 2.b shows same image as Figure 2.a except observed at 07Z on December 23, 1987. Figure 3 is regional analyses of SST at a grid interval of .5 latitude by .5 longitude for the region same as Figure 2.a from the 2-channel SST algorithm of this study. For comparison with ship measurements, ship observed SST are also shown in Figure 3 by number in circle. The largest time difference between ship report and satellite observation is about 1 day. The results of the satellite-derived SST and ship measured SST matchups are shown in Table 3 on an individual basis. During this time, The 2-channel SST algorithm of using this cloud-clearing technique had a bias of .2875°C and a RMSE of .9198 °C. This low value of RMSE closes to the clear region result and most encouraging.

For additional test, satellite measurement at 07Z on December 23, 1987 is also chosen to estimate SST. Figure 4 is regional analyses of SST same as Figure 3 except on December 23. Comparing the regional analyses of SST with ship reports (number in circle), one can see that the satellite-derived SST still can catch the ship measurements. The matchups on an individual basis are shown in Table 4. A 2.6 °C SST difference is found at the location of 26.4N, 121.2E. Because ship measurement time at this location is a day earlier than satellite observation time and larger SST gradient is found in this area, these may cause the large SST difference. However, it still had a low bias of .59°C and a low RMSE of 1.0549°C.

Combining these two cases, the satellite-derived SST had a bias of .4556°C and a RMSE of 1.0084°C in comparing with ship measurements.

5. Conclusions and Recommendations

A satellite-derived SST algorithm using AVHRR infrared window data in cloudy area has been developed. Results of the case studies conducted here clearly demonstrate the accuracy of satellite-derived SST under partly cloudy conditions. However, it is difficult to quantify the real accuracy provided by this method since the ship measured SST are not error free. Studies of buoy versus ship observations of SST have shown that ship measurements are $.2 \pm 1.5$ °C greater than those of buoys (Tabata, 1978). Besides, ship and satellite observations are rarely taken at the same time.

The multichannel SST algorithm derived by Tseng was based on the simulated data. So algorithm construct from the real satellite and ship measurements may be needed to increase the potential improvement.

Although the results of this study have been very encouraging, more comparisons between the satellite-derived and ship measured SST in cloudy regions should be done to qualify the usefulness of this method.

References:

1. Bates, J. J., 1982: Sea Surface Temperature Derived from VAS Multispectral Data. M.S. Thesis, Department of Meteorology, University of Wisconsin, Madison, Wisconsin, 40pp.

2. Coakley, J. A., F. P. Bretherton, 1982: Cloud Cover from High-Resolution scanner Data: Detecting and Allowing for Partially Filled Fields of View. *J. Geophys. Res.*, 87, 4917-4932.
3. McClain, E. P., 1980: Multiple Atmospheric-Window Techniques for Satellite-derived Sea Surface Temperatures. *Oceanography from Space*, Plenum Press, New York, 73-85.
4. Prabhakara, C., G. Dalu, and V. G. Kunde, 1974: Estimation of Sea Surface Temperature from Remote Sensing in the 11 to 13 μ m Window Region. *J. Geophys. Res.*, 79, 5039-5044.
5. Smith, W. L., P. K. Rao, R. Koffler, and W. R. Curtis, 1970: The Determination of Sea Surface Temperature from Satellite High Resolution Infrared Window Radiation Measurements. *MWR*, 98, 604-611.
6. Tabata, S., 1978: Comparison of Observations of Sea Surface Temperature at Ocean Station P and NOAA Buoy Stations and Those Made by Merchant Ship Traveling in Their Vicinities in the Northeast Pacific Ocean. *J. Applied Meteor.*, XVII, 374-385.
7. Tseng, C. Y., 1986 : Water Vapor Correction of Sea Surface Temperature in Satellite Remote Sensing. Academia Sinica, Taiwan, R.O.C., 37pp.
8. Warnecke, G. L., L. J. Allison, L. McMillin, and K. H. Szekiolda, 1971: Remote Sensing of Ocean Currents and Sea Surface Temperature Changes Derived from the Nimbus II Satellite. *J. Phys. Oceanogr.*, 1, 45-60.

Table 1: Characteristics of AVHRR Channels

Channel	Wavelength (μm)	Primary Uses
1	0.58 - 0.68	daytime cloud/surface mapping
2	0.725 - 1.10	water delineation, ice and snow melt
3	3.55 - 3.93	sea surface temperature, nighttime clouds
4	10.30 - 11.30	sea surface temperature, day/night clouds
5	11.50 - 12.50	sea surface temperature, day/night clouds

Table 2: Multichannel SST algorithm

	A0	A1	A2	A3
2 channels:	-3.738702	3.827533	-2.812222	-
3 channels:	-6.120660	1.001975	0.9285381	-0.9055073

Table 3: Comparison of Satellite-derived and ship measured SST for 07Z December 21, 1987. (in $^{\circ}\text{C}$)

Latitude	Longitude	Ship SST	Satellite SST	Bias
21.7N	119.0E	24.0	24.4	0.4
22.0N	123.1E	25.0	25.9	0.9
24.2N	123.1E	26.0	26.4	0.4
24.3N	125.9E	27.2	27.1	-0.1
26.0N	122.0E	21.0	22.8	1.8
26.1N	120.8E	22.0	20.5	-1.5
26.4N	121.2E	19.0	19.8	0.8
26.5N	123.0E	25.0	24.6	-0.4

Total: N=8, Bias=0.2875, RMSE=0.9198

Table 4: Same as Table 3 except for 07Z December 23, 1987.

Latitude	Longitude	Ship SST	Satellite SST	Bias
20.1N	119.7E	27.0	26.2	-0.8
20.8N	120.9E	24.4	25.3	0.9
21.8N	123.6E	26.0	26.4	0.4
22.0N	124.0E	26.0	26.4	0.4
22.7N	127.9E	28.7	27.7	-1.0
24.3N	125.9E	27.2	27.1	-0.1
26.3N	123.0E	22.5	24.4	1.9
26.4N	121.2E	19.0	21.6	2.6
27.6N	125.1E	21.0	22.1	1.1
28.6N	127.8E	22.2	22.7	0.5

Total: N=10, Bias=0.5900, RMSE=1.0549

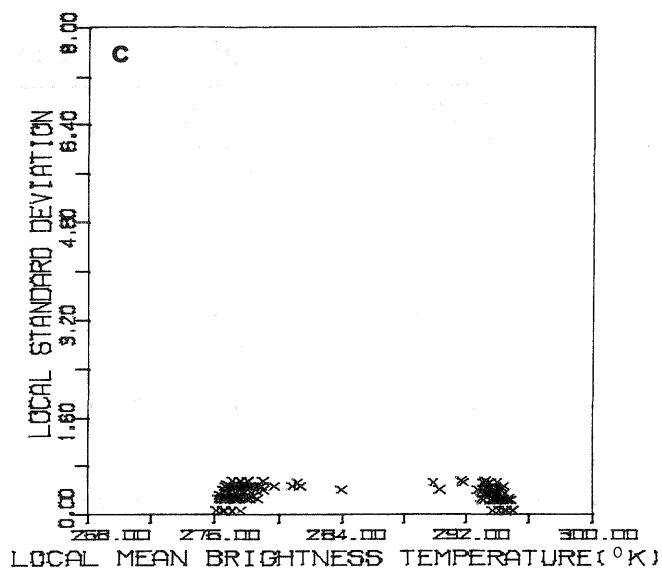
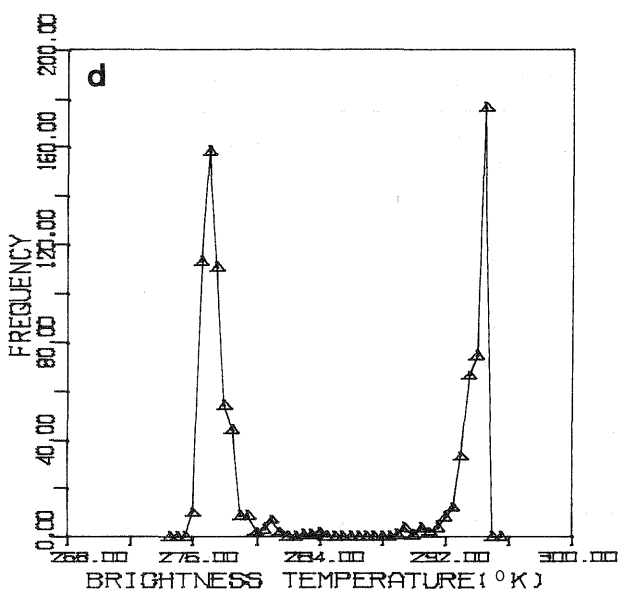
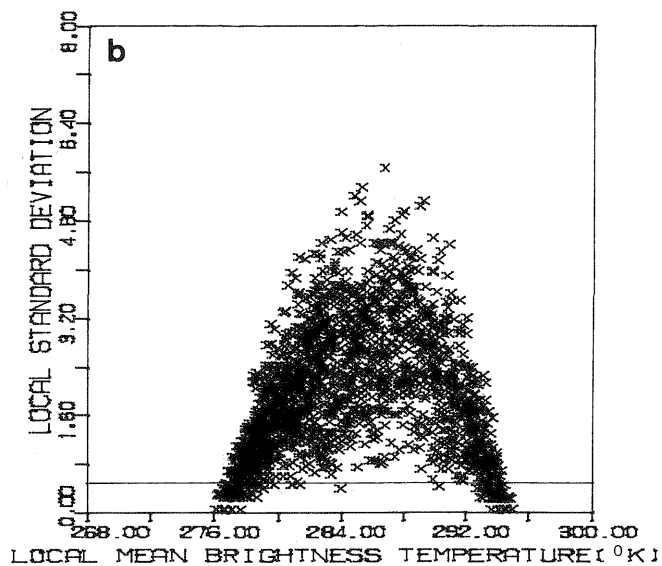
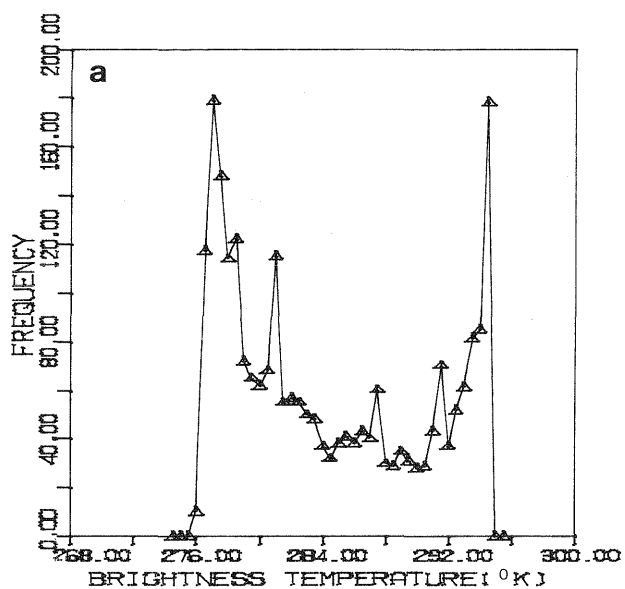
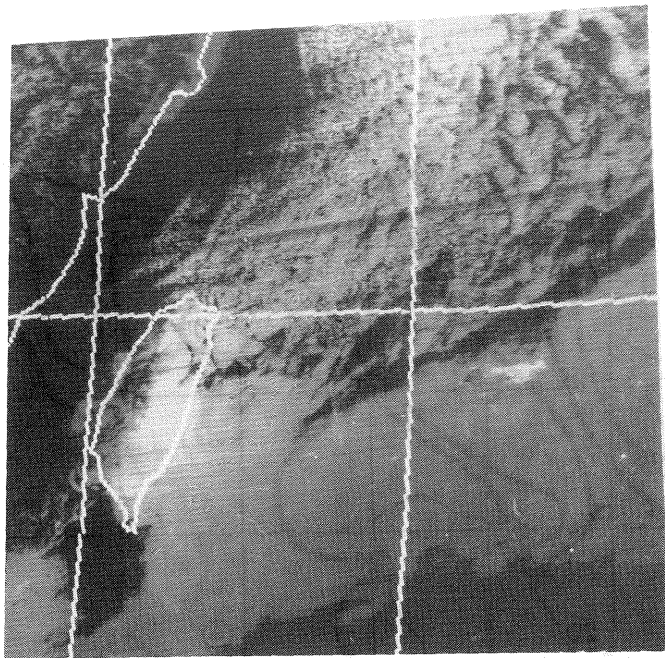
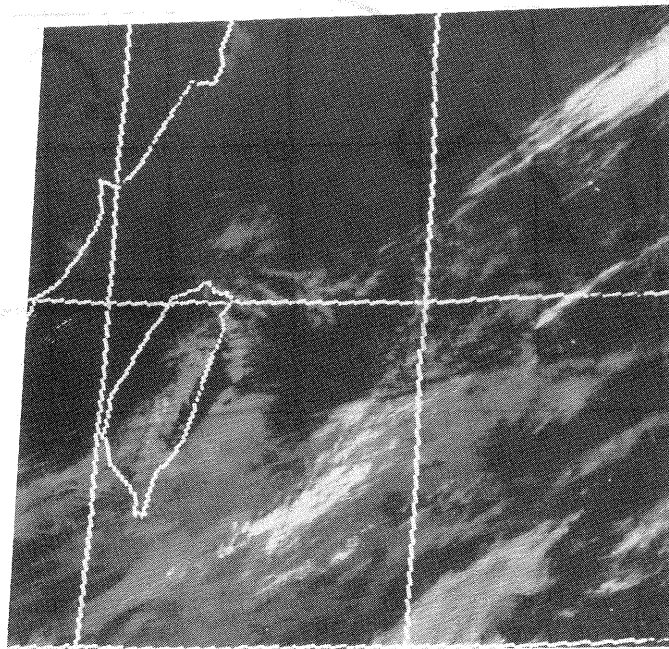


Figure 1: (a) Frequency histogram of AVHRR Channel 4 Brightness temperature for a .5 latitude by .5 longitude region. (b) Local standard deviation as a function of the mean brightness temperature. (c) Same as b. except cut out the points whose local standard deviation is greater than .5. (d) Same as a. except filtering out partially filled spots.



a



b

Figure 2: (a) Image of AVHRR Channel 4 radiances for a region from 20N to 28N and from 118E to 127E at 07Z on December 21, 1987. (b) Same as a. except on December 23, 1987.

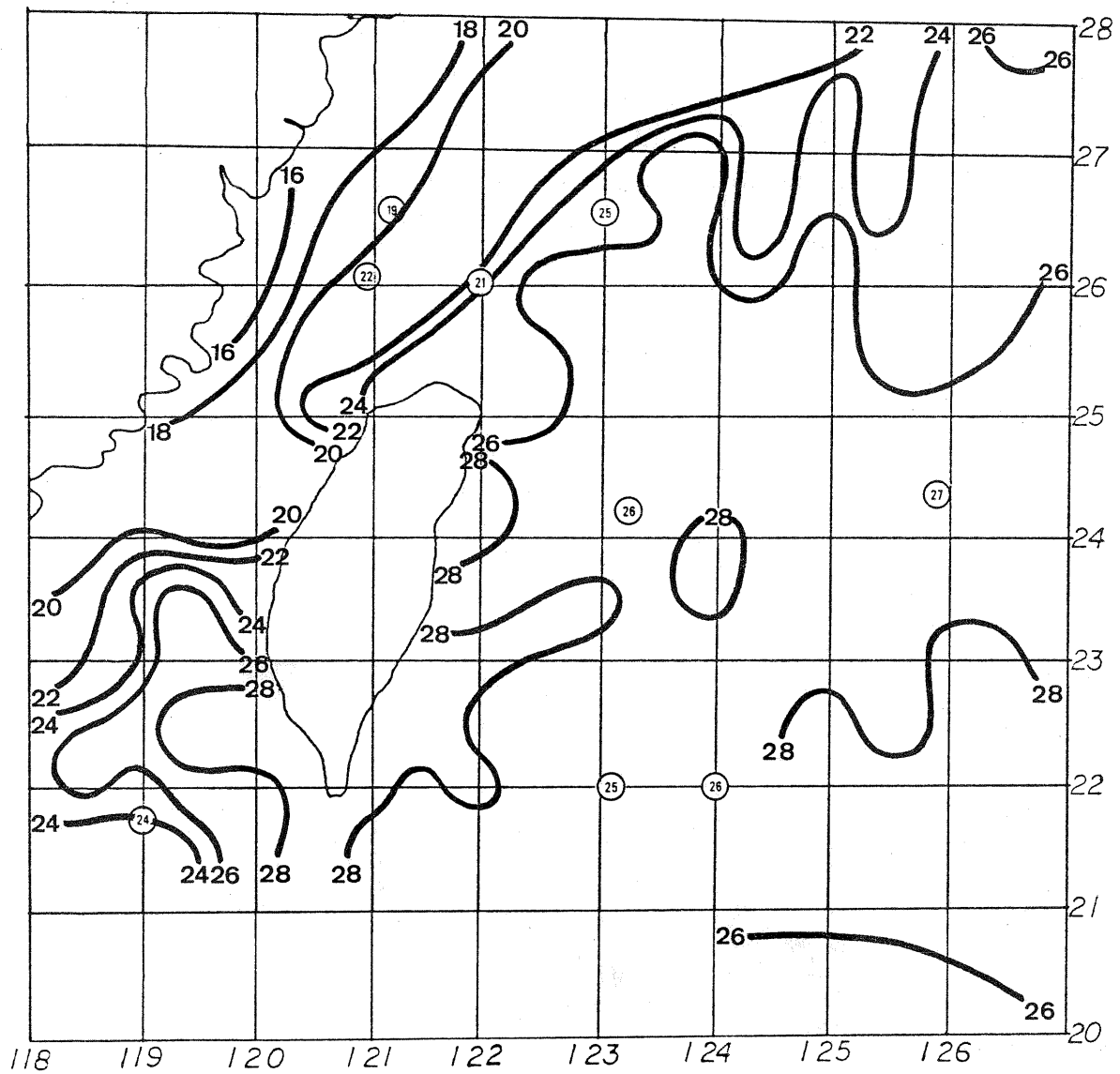


Figure 3: Regional analyses of SST at a grid interval of .5 latitude by .5 longitude at 07Z on December 21, 1987.

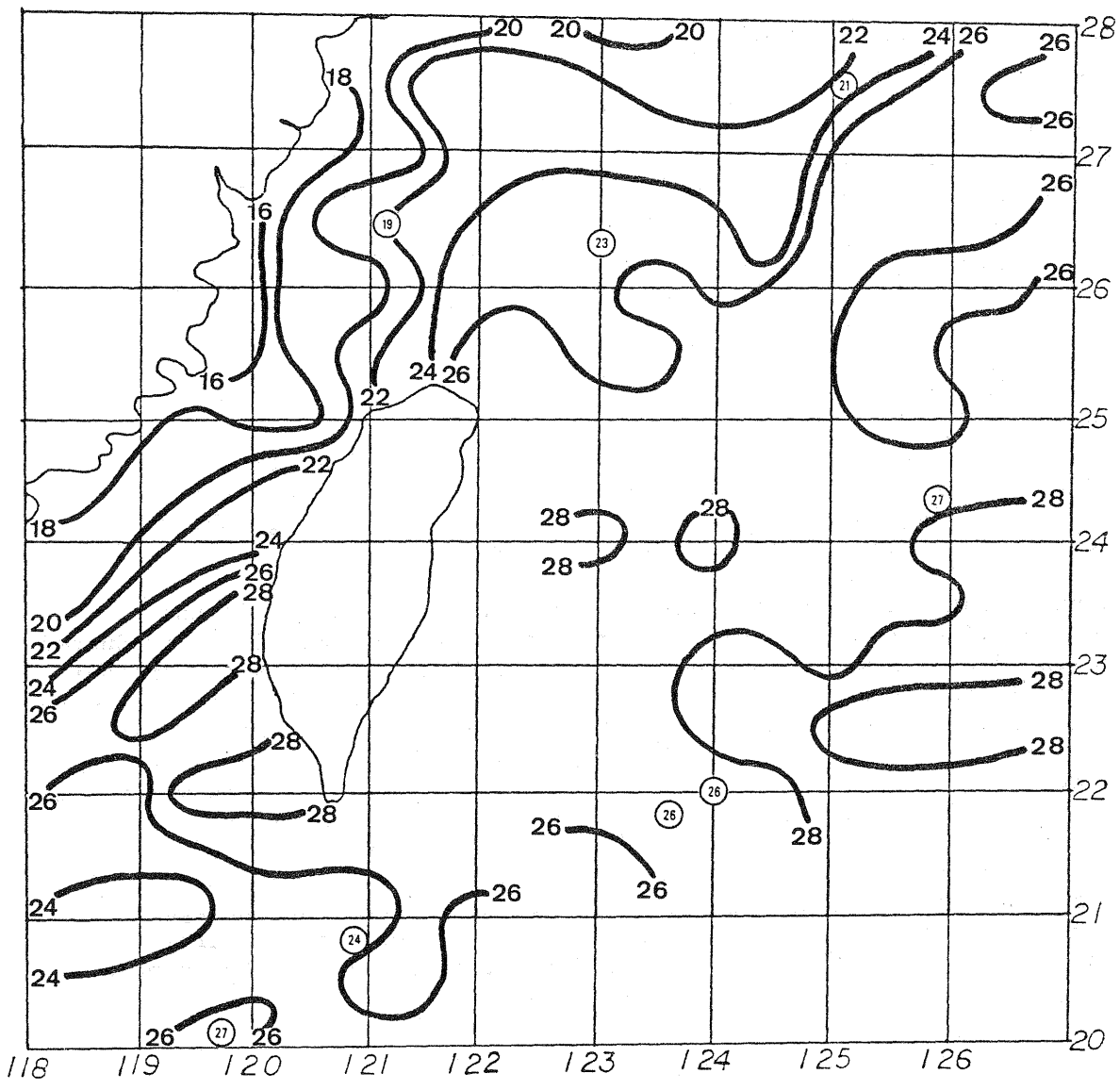


Figure 4: Same as Figure 3 except on December 23, 1987.